

Planning under risk and uncertainty based on Prospect-theoretic models

Aamodh Suresh and Sonia Martínez

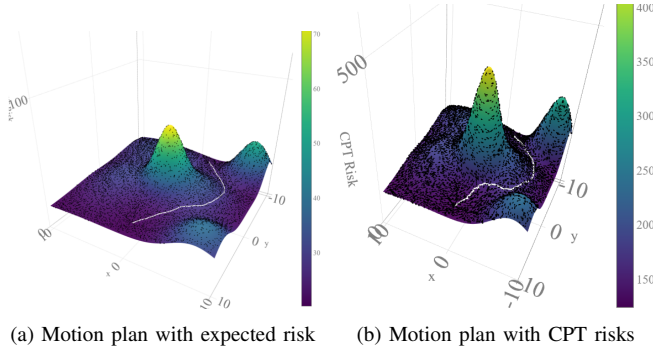


Fig. 1: Environment perception and sampling-based motion planning using a) Rational environment perception using expected risk, b) DM’s Risk-Averse environment perception. The sampled points are indicated as black dots and the path is indicated as a white line.

Abstract—In this work, we develop a novel sampling-based motion planning approach to generate plans in a risky and uncertain environment. To model a variety of risk-sensitivity profiles, we propose an adaption of Cumulative Prospect Theory (CPT) to the setting of path planning. This leads to the definition of a non-rational continuous cost envelope (as well as a continuous uncertainty envelope) associated with an obstacle environment. We use these metrics along with standard costs like path length to formulate path planning problems. Building on RRT*, we then develop a sampling-based motion planner that generates desirable paths from the perspective of a given risk sensitive profile. Since risk sensitivity can greatly vary, we provide a tuning knob to appease a diversity of decision makers (DM), ranging from totally risk-averse to risk-indifferent. Additionally, we adapt a Simultaneous Perturbation Stochastic Approximation (SPSA)-based algorithm to learn the CPT parameters that can best represent a certain DM. Simulations are presented in a 2D environment to evaluate the modeling approach and algorithms’ performance.

I. INTRODUCTION

a) Motivation: Autonomous robots ranging from industrial manipulators to robotic swarms [1], [2], [3], are becoming rapidly ubiquitous and interactive with humans in today’s world. These interactions, whose degree of complexity depends on the human’s involvement in the robot’s workspace, directly affect the robot path-following behavior. This is the case in the simplest scenarios where a decision maker (DM) may participate in the guidance of an autonomous system via shared or supervised control, such as in robotic surgery, search and rescue operations, or autonomous car driving. Arguably, most environments have a degree of risk

and uncertainty associated with the robot’s behavior. In these situations, it becomes imperative for the robot to consider the DM’s perception of the environment to make more cogent motion plans.

Fields like Psycho-physics and Behavioral Economics have studied the human perception of various modalities from physical sensing to monetary risks. Their conclusion is surprisingly similar: humans have a nonlinear perception model governed by power laws [4], [5]. This shows that DMs are often non-rational while making decisions under risk and uncertainty, leading to alternative plans. Motivated by this, we consider a motion planning problem based on a non-rational DM’s perspective, and which differs from that of a fully rational autonomous planning agent. Figure 1 illustrates how a nonlinear DM’s perception of the environment induces a change in the path produced to reach a goal. While Figure 1a shows a rational perception of the environment using expected risk, Figure 1b illustrates a nonlinearly deformed and scaled surface that reflects the risk aversion of a certain DM. In particular, we can observe that the value of the perceived risk is much higher in case of Figure 1b as compared to that of Figure 1a. Here, we study how to adapt Cumulative Prospect Theory (CPT) to embed a DM’s risk aversion characteristics into the motion planning approach. These models, which depend naturally on a set of parameters, are adapted via a learning algorithm to get to a close CPT model that can represent the attitude towards risk of a DM.

b) Related Work: Nonlinear human perception has been studied extensively by the Psychophysics community [6], resulting in the formulation of power law functions to model nonlinear sensations [4]. This has been applied in various engineering fields like speech processing [7], human factors [8], and haptics [9] to design human perception models. Similar power laws have also been employed by the Behavioral Economics community to model human’s perception of risk, as well as uncertainty [10] taking the form of Cumulative Prospect Theory (CPT) [5]. Motivated by this, CPT has been extensively used in numerous engineering applications like traffic routing [11], network protection [12], stochastic optimization [13], and safe shipping policies [14]. However, these notions of nonlinear perception are yet to be applied for general path planning.

Over the past decade, RRT* [15] has been one of the most popular motion planners owing to its asymptotic optimality under certain conditions and the ability to solve complex problems [16]. Risk [17] and uncertainty [18] have been considered for motion planning problems involving a human, but mainly in a probabilistic setting [19] with discrete obsta-

A. Suresh and S. Martínez are with the Department of Mechanical and Aerospace Engineering, University of California at San Diego, La Jolla, CA 92093, USA {aasuresh, soniamd}@eng.ucsd.edu

We gratefully acknowledge support from AFOSR grant FA9550-18-1-0158 and DARPA (Lagrange) N660011824027.

cles. A very few of these works have considered modeling the planning environment with continuous risk maps [20], but considering both risk and uncertainty and modeling their human perception has largely been ignored.

Another challenge arises in the estimation of the nonlinear weighting functions or the CPT parameters when they are unknown [21]. Traditional qualitative methods like surveys [22] and questionnaires [23] along with quantitative statistical tools like Bayesian parameter estimation [24] and Hidden Markov Models [25] have been employed for the CPT parameter estimation and reference point learning problem. But none of these methods address the context of motion planning. However, qualitative methods are not applicable in our case due to the abstract nature of risk involved in planning algorithms, whereas quantitative and efficient methods from data science and statistics are largely inapplicable, due in part to a lack of data and gradient measurements. We have to largely rely on stochastic estimated gradient algorithms like SPSA [26] for estimation. In this context, [27] have utilized SPSA to estimate the CPT parameters for reinforcement learning application, but use a perturbed CPT value function as the loss function which we cannot measure in our case.

c) Contributions: Our contributions lie in three main areas:

- 1) *CPT Environment Generator* :- We propose an adaptation of CPT to generate a DM's nonlinear perception of an environment which is risky and uncertain.
- 2) *CPT Path Planner* :- We generate desirable paths using sampling-based planning on the perceived continuous risky and uncertain environment.
- 3) *CPT Parameter Learner* :- Given a DM's path generated by a CPT-model in a known environment, we learn the CPT parameters that characterize this path by implementing SPSA.

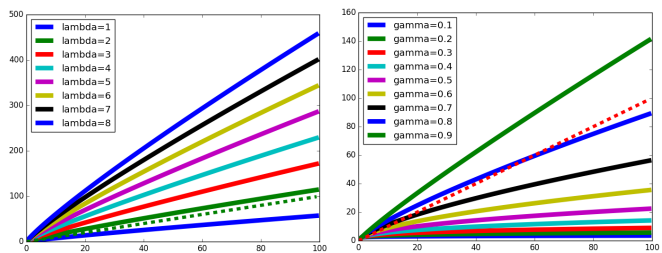
Together with these three aspects, an autonomous agent will be able to learn a specific DM's perception of the environment using CPT models, and be able to generate more relevant future paths to a decision maker. We want to clarify that the validation of the CPT based models with human user studies is not in the current scope of this work.

II. PRELIMINARIES

In this section we will describe the basic notations used in the paper along with a concise description of Cumulative Prospect Theory.

A. Notation

We let \mathbb{R} denote the space of real numbers, $\mathbb{Z}_{\geq 0}$ the space of positive integers and $\mathbb{R}_{\geq 0}$ the space of non negative real numbers. Also, \mathbb{R}^n and $\mathbb{R}^{M \times n}$ denote the n -dimensional real vector space and the space of $M \times n$ real matrices, respectively. We denote $\mathcal{C} \subset \mathbb{R}^n$ as the configuration space used for planning and $\|\cdot\|$ as the Euclidean norm. We use \circ for the composition of two functions f and g , that is $f(g(x)) = f \circ g(x)$. We model a tree by an directed graph $G = (V, E)$, where $V = \{1, \dots, T\}$ denotes the set of sampled points (vertices of the graph), and $E \subset V \times V$, denotes the set of edges of the graph.



(a) Change in risk aversion λ with $\gamma = 0.88$ (b) Change in risk sensitivity γ with $\lambda = 2.25$

Fig. 2: Variation of risk aversion and risk sensitivity. The x-axis indicates the associated risk, ρ , and the y-axis shows the perceived risk, v . The dotted line indicates the line $v = \rho$.

B. Nonlinear risk and uncertainty weighting using CPT

Cumulative Prospect theory [5] is a Nobel prize winning theory, which tries to model human decision making under risk and uncertainty. Traditionally it has been used in the scenario of monetary outcomes like lotteries [5] and stock market [10]. In this section, we adapt it for path planning applications.

The DM is presented with a set of prospects $\{\mathcal{L}^1, \dots, \mathcal{L}^k, \dots, \mathcal{L}^M\}$, with \mathcal{L}^k given by the sequence $\mathcal{L}^k = \{(x^k, \rho_i^k, p_i^k)\}_{i=1}^M$, representing potential risk outcomes and their probabilities associated with the prospect location $x^k \in \mathcal{C}$. More precisely, there are $i \in \{1, \dots, M\}$ possible outcomes by moving to location $x^k \in \mathcal{C}$, and these are given by $\rho_i^k \in \mathbb{R}_{\geq 0}$, a possible risk outcome, which can happen with probability p_i^k . The outcomes are arranged in a decreasing order of risk denoted by $\rho_M < \rho_{M-1} < \dots < \rho_1$ with their corresponding probabilities, such that $\sum_{i=1}^M p_i^k = 1$. As pointed out in Section I, there is significant empirical evidence which suggests that humans in general have a skewed notion of not only the gains and losses but also the probabilities associated with the outcomes.

We can define a utility function, $v: \mathbb{R}_{\geq 0} \rightarrow \mathbb{R}_{\geq 0}$ which represents DM's perceived risk. Also, let us denote $w: [0, 1] \rightarrow [0, 1]$ as the probability weighting function which represents the DM's perception of uncertainty. While previous literature have used various forms for these functions, here we will be consider the CPT value functions v taking the form:

$$v(\rho) = \lambda \cdot \rho^\gamma, \quad (1)$$

where $0 < \gamma < 1$ and $\lambda > 1$. Tversky and Kahnemann suggest the use of $\gamma = 0.88$ and $\lambda = 2.25$ to parametrize an average human in the scenario of monetary lotteries, however this may not hold for our application scenario. The parameter λ represents the coefficient of risk aversion with greater values implying stronger aversion indicative of higher perceived risks, which is indicated in Figure 2a. The parameter γ represents the coefficient of risk sensitivity with lower values implying greater indifference towards risk ρ which is indicated in Figure 2b.

We will be using the popular Prelec's probability weighting function [10], [28] indicative of perceived uncertainty, which takes the form:

$$w(p) = e^{-\beta(-\log p)^\alpha}, \alpha > 0, \beta > 0, w(0) = 0. \quad (2)$$

These concepts illustrate the nonlinear perception of risk and uncertainty and a DM under consideration can be categorized by the parameters $\Theta = \{\alpha, \beta, \gamma, \lambda\}$. We will be using these to construct the DM's perception of a risky and uncertain environment, which will be detailed in Section IV.

III. ENVIRONMENT SETUP AND PROBLEM STATEMENT

In this section, we setup the environment and formulate the problems that we address in the manuscript. To do this, we will consider the case where there is a sense of risk associated with the planning region, as well as uncertainty on this risk.

Suppose we have a mean risk envelope $\rho_\mu : \mathcal{C} \rightarrow \mathbb{R}_{\geq 0}$, and an uncertainty envelope $\rho_\sigma : \mathcal{C} \rightarrow \mathbb{R}_{\geq 0}$ which is the standard deviation of risk associated with each point in the environment. In other words, for each point $x \in \mathcal{C}$ we have a corresponding mean risk $\rho_\mu(x)$ and a standard deviation $\rho_\sigma(x)$ of the distribution of risk profile $\rho(x)$. In the following, we model ρ_μ and ρ_σ as a scaled sum of Bi-variate normal distributions for 2D environments as illustrated in Figure 3a and Figure 3b. With this in mind we will proceed to define the problem statement.

In this paper we propose and solve three main problems:

Problem 1: (CPT Environment Generator). Given the configuration space \mathcal{C} containing a risk envelope ρ_μ and an uncertainty envelope ρ_σ along with the DM's CPT parameters Θ , obtain the DM's perceived risky and uncertain environment \mathcal{C}_{CPT} using CPT.

Problem 2: (CPT Path planner). Given the DM's perceived risky and uncertain environment \mathcal{C}_{CPT} and the start and goal points x_s and x_g compute a desirable path P from x_s to x_g in accordance with the DM's CPT model Θ .

Problem 3: (CPT parameter learner). Given the configuration space \mathcal{C} containing a risk envelope ρ_μ and an uncertainty envelope ρ_σ along with a DM's generated path P_d , according to some CPT model, find the CPT parameters Θ^* of this model.

IV. PERCEIVED ENVIRONMENT GENERATION USING CPT

In this section, we will generate a DM's perceived environment using the notions of CPT developed in Section II-B. Given the environment setup from Section III, we consider the risk associated with the point $x \in \mathcal{C}$ as a random variable $\rho(x)$ belonging to a normal distribution $\mathcal{N}(\rho_\mu(x), \rho_\sigma(x)^2)$ truncated using the 3σ rule of thumb to describe the support of the distribution. So we have $\rho(x) \in [\rho_\mu(x) - 3\rho_\sigma(x), \rho_\mu(x) + 3\rho_\sigma(x)]$, which accounting for about 99.7% of the risk values. For simplicity, we use a discrete approximation of this distribution by considering number of bins $M \in \mathbb{Z}_{\geq 0}$, to obtain a set of possible risk values $\rho(x) \triangleq \{\rho_1(x), \dots, \rho_M(x)\}$ with

$$\rho_i(x) = \rho_\mu(x) - 3\rho_\sigma(x) + \frac{6i\rho_\sigma(x)}{M}, \quad i \in \{1, \dots, M\} \quad (3)$$

and their corresponding probabilities $p(x) \triangleq \{p_1(x), \dots, p_M(x)\}$ such that $p_i(x_1) = p_i(x_2)$, $\forall x_1, x_2 \in \mathcal{C}$ and $i \in \{1, \dots, M\}$

Now, the expected Risk $R(x)$ associated with a point x is

$$R(x) = \frac{1}{M} \sum_{i=1}^M \rho_i(x) p_i(x). \quad (4)$$

That is, from (4) we have an expected risk envelope $R : \mathcal{C} \rightarrow \mathbb{R}_{\geq 0}$ which is shown in Figure 3c, associated with the configuration space.

To model the nonrational perception of the expected risk $R(x)$, by a DM, we use the CPT notions developed in Section II-B. Given a set of K points $\{x^1, \dots, x^K\}$ with $x^k \in \mathcal{C}$, the set of prospects can be constructed as $\mathcal{L}^k := \{x^k, \rho_i(x^k), p_i(x^k)\}$, where $i \in \{1, \dots, M\}$ and $k \in \{1, \dots, K\}$.

According to CPT [5], there is a notion of cumulative decision-weight functions $\Pi := \{\pi_1, \dots, \pi_M\}$ which represent the human perception of the probabilities $p_i(x)$ in a cumulative fashion. Define a partial sum function $S_j(p_1, \dots, p_M) \triangleq \sum_{i=j}^M p_i$, then we have

$$\pi_j = w \circ S_j(p_1, \dots, p_M) - w \circ S_{j+1}(p_1, \dots, p_M), \quad (5)$$

where we employ the weighting function w from (2).

With this, a DM expected risk envelope $R^h : \mathcal{C} \rightarrow \mathbb{R}_{\geq 0}$ according to CPT is given by:

$$R^h(x^k) = \frac{1}{M} \sum_{j=1}^M (v \circ \rho_j(x^k)) (\pi_j \circ p(x^k)). \quad (6)$$

Algorithm 1: CPT Environment generator

- 1 Input: \mathcal{C} , $\rho_\mu(x)$, $\rho_\sigma(x)$, Θ
 - 2 Output : \mathcal{C}_{CPT}
 - 3 **for** $x \in \mathcal{C}$ **do**
 - 4 $(\rho(x), p(x)) \leftarrow \mathcal{N}(\rho_\mu(x), \rho_\sigma(x)^2, M)$;
 - 5 $w \circ p(x) \leftarrow e^{-\beta(-\log \circ p(x))^\alpha}$;
 - 6 $v \circ \rho(x) \leftarrow \lambda(\rho(x))^\gamma$;
 - 7 **for** $j \in \{1, \dots, M\}$ **do**
 - 8 $\pi_j \leftarrow w \circ S_j(p_1, \dots, p_M) - w \circ S_{j+1}(p_1, \dots, p_M)$;
 - 9 **end**
 - 10 $R^h(x) \leftarrow \frac{1}{M} \sum_{j=1}^M (v \circ \rho_j(x)) (\pi_j \circ p(x))$;
 - 11 $R(x) \leftarrow \frac{1}{M} \sum_{i=1}^M \rho_i(x) p_i(x)$;
 - 12 **end**
 - 13 $\mathcal{C}_{CPT} \leftarrow \{\mathcal{C}, R(x), R^h(x)\}$
-

These concepts are illustrated in Figure 3, where given a risk envelope across an environment (Figure 3a) and uncertainty (Figure 3b), the DM's perception can vary from being rational (i.e. using expected risk in Figure 3c) to risk averse (Figure 3d) and risk indifferent (Figure 3e). We also note that both functions R and R^h are differentiable, which will be used for the analysis in Section V.

This process gives us the new configuration space \mathcal{C}_{CPT} which is given by $\mathcal{C}_{CPT} = \{\mathcal{C}, R(x), R^h(x)\}$. The entire process is summarized in Algorithm 1. The new space contains the human expected risk envelope $R^h(x)$ and the expected risk envelope $R(x)$ for each point $x \in \mathcal{C}$, which is used for planning in the following section.

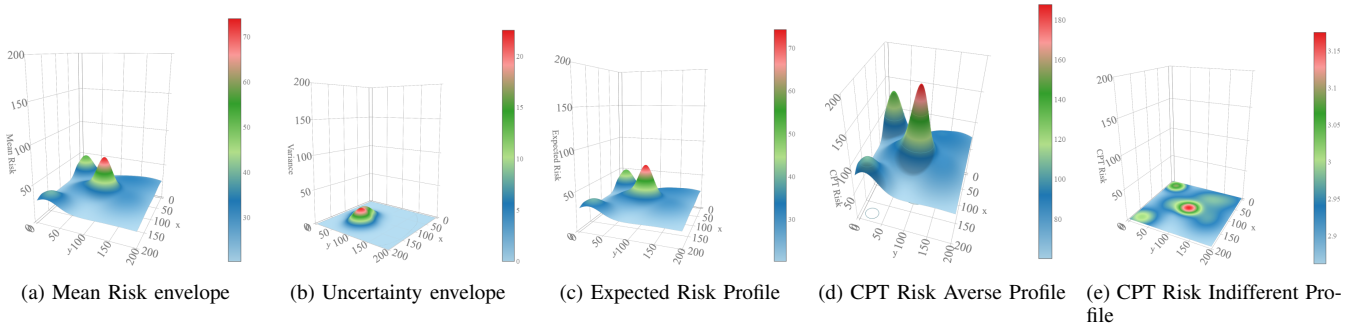


Fig. 3: Environment perception with various modalities.

V. SAMPLING-BASED PLANNER

Here we will use CPT notions to formulate a new cost metric, which will be used for planning in the DM's perceived environment generated in Section IV. In traditional RRT* optimal planning is achieved using path length as the metric. In our setting, the notion of path length is insufficient as it does not capture the risk and uncertainty in the configuration space. We are interested in finding the cost associated with a path P which takes into account risk, uncertainty as well as the path length.

Let two points $x, y \in \mathcal{C}$ be arbitrarily close. A decrease in risk is a desirable trait, hence it is reasonable to add an additional term in the cost only if $R^h(y) - R^h(x) \geq 0$, which indicates an increase in DM's expected risk by traveling from x to y . Consider the set of parameterized paths $\mathcal{P}(\mathcal{C}) \triangleq \{\eta : [0, 1] \rightarrow \mathcal{C} \mid \eta(0) = x, \eta(1) = y\}$. First, we first define the cost $c^h : \mathcal{P}(\mathcal{C}) \rightarrow \mathbb{R}_{\geq 0}$ of a path $\eta \in \mathcal{P}(\mathcal{C})$. Consider a discretization of $[0, 1]$ given by $\{0, t_1, t_2, \dots, t_L = 1\}$ with $t_{\ell+1} - t_\ell = \Delta t$, for all ℓ . Then, a discrete approximation of the cost over η should be:

$$\begin{aligned} c^h(\eta) &\approx \sum_{\ell=1}^L \max\{0, R^h(t_{\ell+1}) - R^h(t_\ell)\} + \delta L(\eta) \\ &= \Delta t \sum_{\ell=1}^L \max\{0, \frac{R^h(\eta(t_{\ell+1})) - R^h(\eta(t_\ell))}{\Delta t}\} + \delta L(\eta), \end{aligned}$$

where $L(\eta)$ denotes the arc-length of the curve η , and $\delta \in \mathbb{R}_{\geq 0}$ is a constant with lower δ representing greater emphasis on the risk profile over path length. This can be tuned to adjust to a specific environment or DM's need. By taking limits in the previous expression, and due to the continuity and integrability of the max operation:

$$\begin{aligned} c^h(\eta) &= \lim_{\Delta t \rightarrow 0} \Delta t \sum_{\ell=1}^L \max\{0, \frac{R^h(\eta(t_{\ell+1})) - R^h(\eta(t_\ell))}{\Delta t}\} + \delta L(\eta) \\ &= \int_0^1 \max\{0, \frac{d}{dt}(R^h(\eta(t)))\} dt + \delta L(\eta) = \\ &= \int_0^1 \max\{0, (R^h)'(\eta(t)) \cdot \eta'(t)\} dt + \delta L(\eta). \end{aligned} \quad (7)$$

From here, the cost of traveling from x to y is given by

$$c^h(x, y) \triangleq \min_{\eta \in \mathcal{P}(\mathcal{C}) : \eta(0)=x, \eta(1)=y} c^h(\eta).$$

Similarly, we define $c : \mathcal{P}(\mathcal{C}) \rightarrow \mathbb{R}_{\geq 0}$ over parameterized paths η (resp. of traveling from x to y in \mathcal{C}) as the cost

$$\begin{aligned} c(\eta) &= \int_0^1 \max\{0, R'(\eta(t)) \cdot \eta'(t)\} dt + \delta L(\eta), \quad (8) \\ c(x, y) &= \min_{\eta \in \mathcal{P}(\mathcal{C}) : \eta(0)=x, \eta(1)=y} c(\eta), \end{aligned}$$

where $R(x)$ is the expected risk calculated at x according to (4) and $\delta \in \mathbb{R}_{\geq 0}$ is a constant.

Remark 1: (Monotonicity). The costs (7) and (8) satisfy monotonic properties in the sense that 1) they assign a positive cost to any path in $\mathcal{P}(\mathcal{C})$, and 2) given two paths η_1 and η_2 , and their concatenation $\eta_2 | \eta_1$, in the space $\mathcal{P}(\mathcal{C})$, it holds that $c^h(\eta_1) \leq c^h(\eta_1 | \eta_2)$ (resp. $c(\eta_1) \leq c(\eta_1 | \eta_2)$), (due to the additive property of the integrals) and 3) c^h (resp. c) are bounded over a bounded \mathcal{C} .

A. Proposed Algorithm

Given \mathcal{C}_{CPT} , a number of iterations T and a start point $x_s \in \mathcal{C}$, we wish to produce graph $G(V, E)$, which represents a tree rooted at x_s whose nodes V are sample points in the configuration space and the edges E represent the path between the nodes in V . Let $\text{cost}^h : \mathcal{C} \rightarrow \mathbb{R}_{\geq 0}$ be a function that maps $x \in \mathcal{C}$ to the cumulative cost to reach a point x from the root x_s of the tree $G(V, E)$ using the CPT cost metric (7). Similarly we define $\text{cost} : \mathcal{C} \rightarrow \mathbb{R}_{\geq 0}$ for the expected cost metric (8).

Remark 2: (Additivity). The cumulative costs cost^h and cost are additive with respect to costs (7) and (8) in the sense that: for any $x \in V$ we have $\text{cost}^h(x) = \text{cost}^h(\text{Parent}(x)) + c^h(\text{Parent}(x), x)$ and similarly $\text{cost}(x) = \text{cost}(\text{Parent}(x)) + c(\text{Parent}(x), x)$.

The other basic functional components of our algorithm CPT-RRT* (Algorithm 2) are briefly explained as follows:

- *Sample()*: Returns a pseudo-random sample $x \in \mathcal{C}$ drawn from a uniform distribution across \mathcal{C} .
- *Nearest(G, x)*: Returns the nearest node according to the Euclidean distance metric from x in tree G .
- *Steer(x_1, x_2)* returns

$$\begin{cases} x_2, & \text{if } \|x_2 - x_1\| \leq d \\ x_1 + d \frac{x_2 - x_1}{\|x_2 - x_1\|}, & \text{otherwise.} \end{cases}$$

- *Near(G, x, γ_{RRT^*}, d)*: returns a set of nodes $X \in V$ around x , which are within a radius as given in [15].

Algorithm 2: CPT-RRT*

```
1 Input:  $T, x_s, x_g, \mathcal{C}_{CPT}$ 
2 Output :  $G(V, E), P$ 
3  $V \leftarrow x_s, E \leftarrow \emptyset, cost^h(x_s) \leftarrow 0;$ 
4 for  $i \in \{1, \dots, T\}$  do
5    $G \leftarrow (V, E);$ 
6    $x_{rand} \leftarrow Sample();$ 
7    $x_{nearest} \leftarrow Nearest(G, x_{rand});$ 
8    $x_{new} \leftarrow Steer(x_{nearest}, x_{rand});$ 
9    $V \leftarrow V \cup x_{new};$ 
10   $x_{min} \leftarrow x_{nearest};$ 
11   $X_{near} \leftarrow Near(G, x_{new}, \gamma_{RRT^*}, d);$ 
12   $c_{min} \leftarrow cost^h(x_{nearest}) + c^h(x_{nearest}, x_{new});$ 
13  for  $x_{near} \in X_{near}$  do
14     $c' \leftarrow cost^h(x_{near}) + c^h(x_{near}, x_{new});$ 
15    if  $c' < c_{min}$  then
16       $x_{min} \leftarrow x_{near};$ 
17       $c_{min} \leftarrow c';$ 
18    end
19  end
20   $cost(x_{new}) \leftarrow c_{min};$ 
21  for  $x_{near} \in X_{near}$  do
22     $c' \leftarrow cost^h(x_{new}) + c^h(x_{new}, x_{near});$ 
23    if  $c' < cost^h(x_{near})$  then
24       $x_{par} \leftarrow Parent(x_{near}, G);$ 
25       $E \leftarrow E(\{x_{par}, x_{near}\}) \cup (\{x_{new}, x_{near}\});$ 
26       $X_{chld} \leftarrow Children(x_{near}, G);$ 
27      for  $x_{chld} \in X_{chld}$  do
28         $cost^h(x_{chld}) \leftarrow cost^h(x_{chld}) -$ 
29           $cost^h(x_{near}) + c'$ 
30      end
31       $cost^h(x_{near}) \leftarrow c'$ 
32    end
33  end
34  $P \leftarrow Path(G, x_s, x_g)$ 
```

- $Parent(x, G)$: Returns the parent node of x in the tree G .
- $Children(x, G)$: Returns the list of children of x in the tree G .
- $Path(G, x_s, x_g)$: Returns the path from the nearest node to x_g in G to x_s . It first uses the $Nearest(G, x_g)$ function, and then applies $Parent(x, G)$ function recursively to obtain path from x_s to the node nearest to x_g .

We note that in order to compute c^h and c for each path, we approximate the cost as the sum of costs over its edges, (x_1, x_2) , and for each edge we compute the cost as the differences $\max\{0, R^h(x_2) - R^h(x_1)\} + \delta L(x_1, x_2)$, where the latter is just the length of the edge. Then, this approximation will approach the computation of the real cost in the limit as the number of samples goes to infinity.

Our proposed CPT-RRT* algorithm varies with respect to RRT* in the following aspects: we consider a general continuous cost profile which leads to no obstacle collision checking, saving computation power which is considerable

for complex high dimensional space. We also consider both path length and CPT costs for choosing parents and rewiring with the parameter δ which serves as relative weighting between CPT costs and euclidean path length.

Remark 3: (ER-RRT).* We can obtain the expected risk version of Algorithm 2 by replacing cost function c^h by c from (8) and following the same procedure as Algorithm 2. The results are visualized in Figure 1a.

Lemma 1: (Asymptotic Optimality). Assuming compactness of \mathcal{C} and the choice of γ_{RRT^*} according to Theorem 38 in [15], the CPT-RRT* algorithm is asymptotically optimal.

Proof: It follows from the application of Theorem 38 in [15], and the conditions required for the result to hold. More precisely, the cost functions are monotonic (which follows from Remark 1), it holds that $c(\eta) = 0$ iff η reduces to a single point (resp. the same for c^h), and the cost of any path is bounded. The latter follows from the compactness of \mathcal{C} and continuity of the cost functions. In addition, the costs are also of cumulative nature, due to the additivity property in Remark 2. Finally, the result also requires the condition of the zero measure of the set of points of an optimal trajectory. The holds because both costs include a term for path length. ■

Simulation results of CPT-RRT* algorithm are presented in Section VII-A. To complete the framework, we present a learning algorithm to obtain a DM's CPT profile next.

VI. LEARNING THE CPT PARAMETERS

In the previous sections we have explained how to plan a risk sensitive path using our algorithm CPT-RRT*, detailed in Algorithm 2. Since the decision maker's CPT model can vary greatly, we propose here the use of a learning algorithm to adjust the CPT parameters Θ , in order to generate better quality paths corresponding to the specific CPT profile.

Let us suppose that a decision maker has a particular set of parameters Θ_d , which we wish to use in the path planning problem, but this set Θ_d is unknown. To learn these parameters, one can employ a loss function $J: \Theta \rightarrow \mathbb{R}_{\geq 0}$, where Θ is the space for all sets of parameters Θ introduced in Section II-B, and such that $J(\Theta) = 0 \iff \Theta = \Theta_d$ and $J(\Theta) > 0 \forall \Theta \neq \Theta_d$. The natural choice of J would be the value of an optimal path joining a start and a goal position, which depends on the parameters Θ . However, we have neither access to the values of $J(\Theta)$, as is the solution of the planning algorithm, nor to its gradient. We only have access to the paths P_d generated from the decision maker's CPT profile. In the sequel, we will discuss how to employ SPSA [26] to arrive at a candidate Θ describing the CPT profile of the given path P_d .

A. Learning with SPSA

Our starting point is a generated path P_d for which we need to find the parameter Θ . We would like to measure $y(\Theta) = \|P_\Theta - P_d\|$ corresponding to the distance between the generated path P_d and the (optimal) path P_Θ generated the parameter Θ , Considering this we propose Algorithm 3 which follows an iterative process to estimate the parameter Θ_d corresponding to the generated path. Here we will present

the algorithm succinctly and we refer the reader to [29], [26] for more detailed treatment and analysis of the SPSA algorithm.

The idea is to perturb the estimate Θ_k according to Line 7 using a sample vector Δ_k from Line 6 to get perturbations Θ^+ and Θ^- , for the k^{th} iteration. These perturbations are then used to generate the CPT environments $\mathcal{C}_{\Theta^+}, \mathcal{C}_{\Theta^-}$ using Algorithm 1 as in Line 8. These perturbed environments are used to generate the perturbed paths $P_{\Theta^+}, P_{\Theta^-}$ using Algorithm 2 as in Line 9. With these perturbed paths we can take the loss function measurements $y(\Theta^+), y(\Theta^-)$ according to Line 10. Now from Line 11, we can compute the estimated gradient $\hat{g}_k(\Theta_k)$. With $\hat{g}_k(\Theta_k)$, we can update our parameter Θ_k according to Line 12. To test the goodness of the updated parameter we obtain the corresponding path $P_{\Theta_{k+1}}$ and check whether its within tolerance limit $\kappa \in \mathbb{R}_{>0}$, if yes, exit and return Θ_{k+1} , else we proceed for more iterations. We followed the guidelines from [29], [26] for choosing the parameters Δ_k, a_k, c_k with $a_k, c_k > 0$; $a_k, c_k \rightarrow 0$ as $k \rightarrow \infty$ and Δ_k is symmetrically distributed around 0 and $E(\Delta_k^2), E(\Delta_k^2) < \infty$. The results of Algorithm 3, and the specific choice of these parameters are presented and discussed in Section VII-B.

Algorithm 3: CPT SPSA Learner

```

1 Input:  $\mathcal{C}, \rho_\mu(x), \rho_\sigma(x), P_d$ 
2 Output :  $\Theta, P_\Theta$ 
3  $k \leftarrow 0, \Theta_k \leftarrow \{\alpha_0, \beta_0, \gamma_0, \lambda_0\}$ ;
4 while  $k < T_k$  do
5   Compute  $a_k, c_k$ ;
6    $\Delta_k = \text{Sample}()$ ;
7    $\Theta^+ \leftarrow \Theta_k + c_k \Delta_k, \Theta^- \leftarrow \Theta_k - c_k \Delta_k$ ;
8    $\mathcal{C}_{\Theta^+}, \mathcal{C}_{\Theta^-} \leftarrow \text{Algorithm 1}(\text{Input}, \{\Theta^+, \Theta^-\})$ ;
9    $P_{\Theta^+}, P_{\Theta^-} \leftarrow \text{Algorithm 2}(\{\mathcal{C}_{\Theta^+}, \mathcal{C}_{\Theta^-}\})$ ;
10   $y(\Theta^+), y(\Theta^-) \leftarrow \|P_{\Theta^+} - P_d\|, \|P_{\Theta^-} - P_d\|$ ;
11   $\hat{g}_k(\Theta_k) \leftarrow \frac{y(\Theta^+) - y(\Theta^-)}{2c_k \Delta_k}$ ;
12   $\Theta_{k+1} \leftarrow \Theta_k - a_k \hat{g}_k(\Theta_k)$ ;
13   $\mathcal{C}_{\Theta_{k+1}} \leftarrow \text{Algorithm 1}(\mathcal{C}, \rho_\mu(x), \rho_\sigma(x), \Theta_{k+1})$ ;
14   $P_{\Theta_{k+1}} \leftarrow \text{Algorithm 2}(\mathcal{C}_{\Theta_{k+1}})$ ;
15  if  $\|P_d - P_{\Theta_{k+1}}\| < \kappa$  then
16     $\Theta \leftarrow \Theta_{k+1}$ ;
17    Return;
18  end
19   $k \leftarrow k + 1$ 
20 end

```

VII. RESULTS AND DISCUSSION

In this section we will illustrate the results of the Algorithms proposed in Sections IV, V, and VI. We will use the environment described in Section IV shown in Figure 3.

A. Environment Perception and Planning

We investigate the results of the CPT Environment generator Algorithm and CPT-RRT* Algorithm for solving Problem 1 and Problem 2.

a) *Setup:* We consider a 2D configuration space $\mathcal{C} = [-10, 10] \times [-10, 10]$, with a risk envelope ρ_μ and uncertainty envelope ρ_σ constructed as a scaled sum of normal distributions as shown in Figures 3a and 3b. For ρ_μ we used a set of 7 bi-variate Normal distributions with means $[\mu_r]_{i=1}^7 = \{(-4, 0), (2, -6), (5.5, 2), (-8, 8), (8, -8), (0, 0), (-8, -8)\}$ and their set of corresponding covariance matrices $[\Sigma_r]_{i=1}^7 = \left\{ \begin{pmatrix} 8.5 & 0 \\ 0 & 8.5 \end{pmatrix}, \begin{pmatrix} 12.5 & 0 \\ 0 & 9.5 \end{pmatrix}, \begin{pmatrix} 9.5 & 0 \\ 0 & 12.5 \end{pmatrix}, \begin{pmatrix} 6.5 & 0 \\ 0 & 5.5 \end{pmatrix}, \begin{pmatrix} 12.5 & 0 \\ 0 & 15.5 \end{pmatrix}, \begin{pmatrix} 2.5 & 0 \\ 0 & 2.5 \end{pmatrix}, \begin{pmatrix} 3.5 & 0 \\ 0 & 3.5 \end{pmatrix} \right\}$. We then obtained their normalized sum and scaled it by a factor of 5000 to obtain the final ρ_μ distribution over \mathcal{C} shown in Figures 3a. For the uncertainty envelope we use 2 bi-variate Normal distributions with means $[\mu_u]_{i=1}^2 = \{(-4, 0), (-2, -4)\}$ and their set of corresponding covariance matrices $[\Sigma_u]_{i=1}^2 = \left\{ \begin{pmatrix} 4.5 & 0 \\ 0 & 4.5 \end{pmatrix}, \begin{pmatrix} 3.5 & 0 \\ 0 & 3.5 \end{pmatrix} \right\}$. We then obtained their normalized sum and scaled it by a factor of 300 to obtain the final ρ_μ distribution over \mathcal{C} shown in Figures 3a. Similarly we used For the CPT parameters Θ , we consider fixing $\alpha = 0.74$ and $\beta = 1$, since the corresponding probabilities are the same for each point $x \in \mathcal{C}$ according to Section IV. We use a bin size $M = 20$ to discretize the distributions at each point. We also added a constant factor to ρ_μ to make sure the resulting risk values ρ_i^k remain positive. We consider $T = 20,000$ iterations for the CPT-RRT* Algorithm with a stepsize $d = 0.4$ units and $\gamma_{\text{RRT}^*} = 50$. We have taken $\delta = 1$ to compute c^h and c in CPT-RRT* and ER-RRT* respectively.

b) *Simulations:* The simulation results of using Algorithm 1 and Algorithm 2 are included here using the setup described in the previous paragraph with fixed $x_s = [0, 8]$ and $x_g = [-2, -8]$. First, we fix $\lambda = 2.25$, then we vary γ as illustrated in Figure 4, the CPT-RRT* tree is indicated as white lines and the final path produced is indicated in red. We see that the behavior is as expected, and with decrease in γ , the risk sensitivity decreases. We see that, in the cases where risk sensitivity is low when $\gamma = 0.28, 0.18$, the CPT-RRT* paths is almost a straight line indicating the indifference towards the risk profile of the DM. Whereas, in cases when $\gamma = 0.88$ we see that the CPT-RRT* Algorithm avoids the high risk area in the center, indicating sensitivity towards risk. Now we fix $\gamma = 0.88$ and check the results of variation of λ in the perceived environment and the path produced. Figure 5 indicates the results, which shows that increase in γ corresponds to increase in risk aversion, confirming our expectations. With higher risk aversion with $\gamma = 5.5$ we see a longer and curvier path taken to avoid the central high risk area. Whereas, when $\gamma = 2.0$, we see a shorter path closer to the central region which is consistent with a lower risk aversion.

c) *Discussion:* We have showed that the risk aversion factor λ and risk sensitivity factor γ can be tuned to produce paths describing varying risk profiles. Although a particular profile is shown in Figure 4 and Figure 5, we noted similar behavior with alternative start and goal points. We note the path smoothness is enhanced with higher iterations T , due to asymptotic properties of CPT-RRT* algorithm. We recommend upwards of $T = 10,000$ iterations to achieve

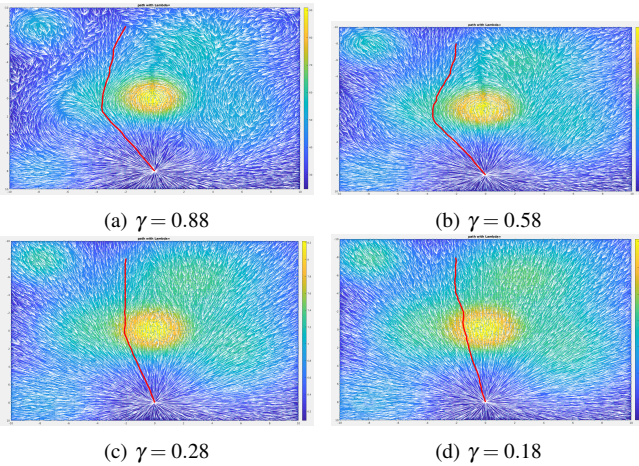


Fig. 4: Path variation with the change of γ , representing the change in perception of risk.

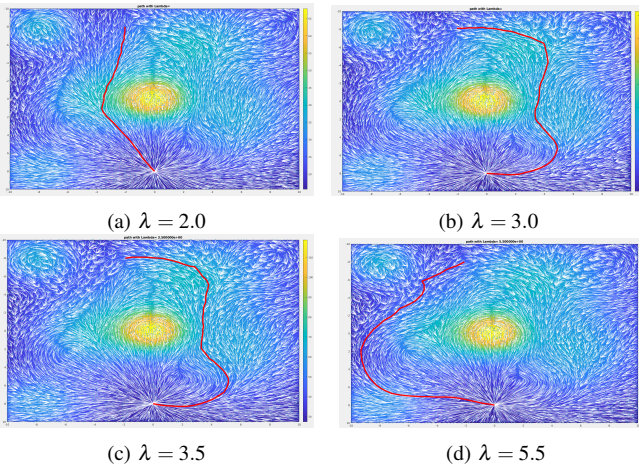


Fig. 5: Path variation with the change of λ , representing the change in loss aversion.

smooth paths in our setting. We also note that the iterations are faster compared to a traditional RRT* pipeline as there is no obstacle checking involved, which saves significant time in complex spaces. From Figures 4, 5, it can be noted that flatter sections (areas with almost constant risk profiles) in the environment can produce similar paths for different Θ , so non-flat environments are needed to capture the essence of nonlinear perception among DM. Future work will be devoted to the analysis of how non-flat environments lead to a clearer distinction of paths with varying the CPT parameters. Overall, our adaptation of CPT to the planning setting seems to produce paths that are consistent with a given risk scenario.

B. Learning the CPT parameters

We now discuss the proposed CPT SPSA framework of Section VI-A to learn the parameters Θ of a path P_d .

a) Setup: We will use the same \mathcal{C} , risk profile ρ_μ and uncertainty profile ρ_σ from Figure 3. Following guidelines from [29], we consider a Bernoulli distribution of Δ_k with support $\{-1, 1\}$ and equal probabilities, learning rate

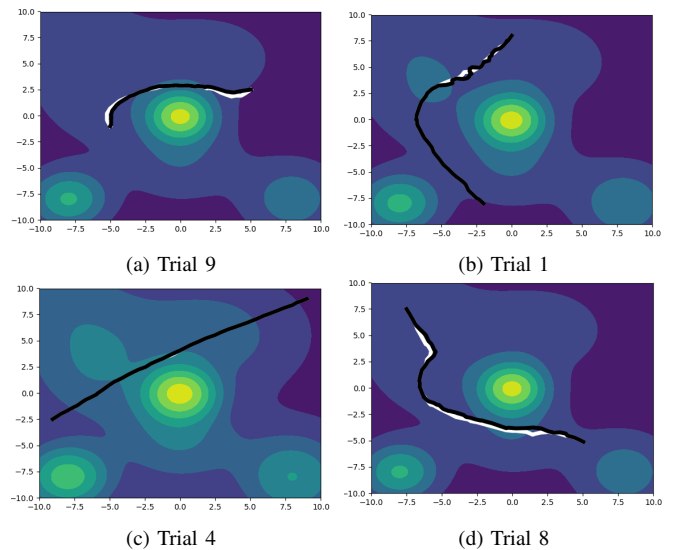


Fig. 6: Path comparison of a given path (white) and computed by SPSA (Black of a few selected cases from Table 1).

TABLE I: CPT Learner Evaluation.

Sl. no	x_s	x_g	$\Theta_d : \{\gamma, \lambda\}$	$\ P_d - P_\Theta\ $	$\Theta : \{\gamma, \lambda\}$
1	{0, 8}	{-2, -8}	{0.68, 4.5}	4.53	{0.72, 5.09}
2	{0, 8}	{-2, -8}	{0.18, 1.2}	0.43	{0.08, 1.273}
3	{0, 8}	{-2, -8}	{0.88, 6.5}	1.3	{0.98, 6.19}
4	{9, 9}	{-9, -2.5}	{0.18, 1.2}	0.08	{0.082, 1.273}
5	{9, 9}	{-9, -2.5}	{0.68, 4.5}	11.76	{0.98, 3.33}
6	{9, 9}	{-9, -2.5}	{0.88, 6.5}	2.28	{0.91, 5.09}
7	{-7.5, 7.5}	{5, -5}	{0.5, 4}	23	{0.31, 1.85}
8	{-7.5, 7.5}	{5, -5}	{0.8, 6}	8.97	{0.91, 10}
9	{5, 2.5}	{-5, -1}	{0.3, 4.5}	1.77	{0.9, 1.52}
10	{5, 2.5}	{5, -1}	{0.7, 8.5}	0.14	{0.91, 7.22}

$a_k = \frac{0.4}{(1.6+k)^{0.601}}$ and perturbation parameter $c_k = \frac{0.97}{(1.6+k)^{0.301}}$. We fix $\alpha = 0.74$ and $\beta = 1$ throughout the simulations and we choose $\Theta_0 = \{\gamma_0, \lambda_0\} = \{0.88, 2.25\}$ which are the nominal parameters from [5]. We generate trajectories in this environment using Algorithm 1 and 2 for different initial conditions x_s , x_g , and CPT parameters Θ_d which serve as ground truth. We use P_d which denotes the path generated by parameters Θ_d as input to the proposed SPSA learner in Section VI-A. We then evaluate the estimated parameter Θ from applying Algorithm 3 and compute $\|P_d - P_{\Theta_{k+1}}\|$ which serves as the noisy measurement of the loss function. We use $T_k = 10000$ iterations to implement Algorithm 2.

b) Simulations: We considered 10 different trials to test our proposed learning Algorithm as shown in Table I. We varied the start and goal points: x_s and x_d , and also the parameters γ and λ to generate different paths corresponding to different ground truths. We then used the algorithm proposed in Section VI to generate an estimate of Θ consisting of γ and λ . The results are summarized in Table I and we see that in most cases the predicted path P_Θ and predicted Θ are close to their true counterparts. We get a mean path error $\|P_d - P_\Theta\|$ as 5.426 units with standard deviation 5.97. Not considering the outlier trial 7 we have very good performance with majority of the trials resulting in minimal path errors. Some of the trials are graphically visualized in Figure 6.

c) *Discussion:* We have showed that our proposed CPT SPSA learner estimates a path quite close to the supplied path P_d which is depicted in Figure 6 and detailed in Table I. From Table I we also see that the predicted Θ is quite close to ground truth parameters Θ_d in many cases. We notice an interesting case in Trial 9 where $\|P_d - P_\Theta\|$ is low and yet Θ_d is different from Θ . This can be logically explained as the supplied path has low risk sensitivity γ but high risk aversion λ , whereas the predicted path corresponds to high risk sensitivity and relatively less risk aversion. One can imagine similar paths for these scenarios, resulting in this behavior. Since we used only 10000 iterations for the CPT-RRT* algorithm within the CPT SPSA learner, we see that the predicted curves may not be smooth as illustrated in Trial 1(Figure 6b). This captures the tradeoff between accuracy and computation costs of the proposed algorithm. We also found that the algorithm converges within 10 iterations in most cases. This is because we consider large perturbations c_k , considering the fact that small perturbations may not result in different paths as shown in Section VII-A. Overall our implementation of the SPSA based learning algorithm predicts relevant CPT parameters from the generated path.

VIII. CONCLUSIONS AND FUTURE WORK

In this work, we have proposed a novel adaptation of CPT to model a DM's non-linear perception of an environment which is risky and uncertain in the context of path planning. The approach combines diverse tools from Path Planning, Behavioral Economics, Optimization and Robotics for this purpose. Firstly, we have demonstrated a DM's non-linear perception of a 2D environment embedded with risk and uncertainty using CPT, and we provide a tuning knob to model perceptions ranging from risk averse to risk indifferent. Next, we propose and demonstrate a novel sampling based planner, the CPT-RRT*, which utilizes the DM's perceived environment to plan asymptotically optimal paths, and we show that they vary according to the risk perception of the DM. Finally, we have also developed and illustrated a CPT parameter learner based on SPSA, which uses a path specified by a DM to estimate the most likely CPT parameters which generated the path, in order to complete the framework. Future work will involve the study of CPT as a good approximator of arbitrary paths in the environment, and alternative approaches to learn CPT parameters from conducting user studies.

REFERENCES

- [1] H. Choset, K. M. Lynch, S. Hutchinson, G. Kantor, L. E. Kavraki, and S. Thrun, *Principles of Robot Motion: Theory, Algorithms and Implementations*. The MIT Press, 2005.
- [2] C. Wu, A. Bayen, and A. Mehta, "Stabilizing traffic with autonomous vehicles," in *IEEE Int. Conf. on Robotics and Automation*, 2018, pp. 1–7.
- [3] A. Suresh and S. Martínez, "Gesture-based human-swarm interactions for formation control using interpreters," in *IFAC Conf. on Cyber-Physical and Human System*, Miami, FL, USA, 2018, pp. 83–88.
- [4] S. S. Stevens, "Neural events and the psychophysical law," *Science*, vol. 170, no. 3962, pp. 1043–1050, 1970.
- [5] A. Tversky and D. Kahneman, "Advances in prospect theory: Cumulative representation of uncertainty," *Journal of Risk and Uncertainty*, vol. 5, no. 4, pp. 297–323, 1992.

- [6] S. S. Stevens, "On the psychophysical law," *Psychological Review*, vol. 64, no. 3, pp. 153–181, 1957.
- [7] C. Kim and R. M. Stern, "Feature extraction for robust speech recognition using a power-law nonlinearity and power-bias subtraction," in *Interspeech*, 2009, pp. 28–31.
- [8] M. L. Bolton, "Modeling human perception, could Stevens' Power Law be an emergent feature?" in *IEEE Int. Conf. on Systems, Man and Cybernetics*, 2008, pp. 1073–1078.
- [9] C. Hatzfeld, *Haptics as an Interaction Modality*, ser. Engineering Haptic Devices. Springer, London, 2014.
- [10] S. Dhama, *The Foundations of Behavioral Economic Analysis*. Oxford University press, 2016.
- [11] S. Gao, E. Frejinger, and M. Ben-Akiva, "Adaptive route choices in risky traffic networks: A prospect theory approach," *Transportation Research Part C: Emerging Technologies*, vol. 18, no. 5, pp. 727–740, 2010.
- [12] A. R. Hota and S. Sundaram, "Game-Theoretic Protection against Networked sis Epidemics by Human Decision-Makers," *IFAC Papers Online*, vol. 51, no. 34, pp. 145–150, 2019.
- [13] C. Jie, L. A. Prashanth, M. Fu, S. Marcus, and C. Szepesvari, "Stochastic optimization in a Cumulative Prospect Theory framework," *IEEE Transactions on Automatic Control*, vol. 63, no. 9, pp. 2867–2882, 2018.
- [14] L. Wang, Q. Liu, and T. Yin, "Decision-making of investment in navigation safety improving schemes with application of Cumulative Prospect Theory," *Journal of Risk and Reliability*, vol. 232, no. 6, pp. 710–724, 2018.
- [15] S. Karaman and E. Frazzoli, "Sampling-based algorithms for optimal motion planning," *International Journal of Robotics Research*, vol. 30, no. 7, pp. 846–894, 2011.
- [16] B. Boardman, T. Harden, and S. Martínez, "Limited range spatial load balancing in non-convex environments using sampling-based motion planners," *Autonomous Robots*, 2018, available online.
- [17] W. Chi and M. Q. Meng, "Risk-RRT: A robot motion planning algorithm for the human robot coexisting environment," in *Int. Conf. on Advanced Robotics*, 2017, pp. 583–588.
- [18] B. Englot, T. Shan, S. D. Bopardikar, and A. Speranzon, "Sampling-based min-max uncertainty path planning," in *IEEE Int. Conf. on Decision and Control*, 2016, pp. 6863–6870.
- [19] W. Chi and M. Q. Meng, "Multimodal Probabilistic Model-based planning for Human-Robot Interaction," in *IEEE Int. Conf. on Robotics and Automation*, 2018, pp. 1–9.
- [20] D. Devaurs, T. Simeon, and J. Cortes, "Optimal Path Planning in Complex Cost Spaces with Sampling-based Algorithms," *IEEE Transactions on Automation Sciences and Engineering*, vol. 13, no. 2, pp. 415–424, 2016.
- [21] M. O. Reiger, M. Wang, and T. Hens, "Cognitive models of risky choice: Parameter stability and predictive accuracy of Prospect Theory," *Cognition*, vol. 123, no. 1, pp. 21–32, 2012.
- [22] —, "Estimating Cumulative Prospect Theory parameters from an international survey," *Journal of Theory and Decision*, vol. 82, no. 4, pp. 567–596, 2017.
- [23] L. Jiang and Y. Wang, "A human-computer interface design for quantitative measure of regret theory," *IFAC Papers Online*, vol. 51, no. 34, pp. 15–20, 2019.
- [24] H. Nilsson, J. Rieskamp, and E. J. Wagenmakers, "Hierarchical Bayesian parameter estimation for cumulative prospect theory," *Journal of Mathematical Psychology*, vol. 55, no. 1, pp. 84–93, 2011.
- [25] K. Nar, L. J. Ratliff, and S. Sastry, "Learning Prospect Theory value function and reference point of a sequential decision maker," in *IEEE Int. Conf. on Decision and Control*, 2017, pp. 5770–5775.
- [26] J. C. Spall, "Multivariate stochastic approximation using a simultaneous perturbation gradient approximation," *IEEE Transactions on Automatic Control*, vol. 37, no. 3, pp. 332–341, 1992.
- [27] L. A. Prashanth, C. Jie, M. Fu, S. Marcus, and C. Szepesvari, "Cumulative Prospect Theory meets reinforcement learning: Prediction and control," 2016, pp. 1406–1415.
- [28] D. Prelec, "The probability weighing function," *Econometrica*, vol. 66, no. 3, pp. 497–527, 1998.
- [29] J. C. Spall, *Introduction to Stochastic Search and Optimization*. New York, 2003.